

# How the Continents Deform: The Evidence From Tectonic Geodesy\*

Wayne Thatcher

U.S. Geological Survey, Menlo Park, California 94025; email: thatcher@usgs.gov

Annu. Rev. Earth Planet. Sci. 2009. 37:237–62

First published online as a Review in Advance on  
January 20, 2009

The *Annual Review of Earth and Planetary Sciences* is  
online at earth.annualreviews.org

This article's doi:  
10.1146/annurev.earth.031208.100035

Copyright © 2009 by Annual Reviews.  
All rights reserved

0084-6597/09/0530-0237\$20.00

\*The U.S. Government has the right to retain a  
nonexclusive, royalty-free license in and to any  
copyright covering this paper.

## Key Words

GPS, tectonics, microplates, plate tectonics, continental dynamics

## Abstract

Space geodesy now provides quantitative maps of the surface velocity field within tectonically active regions, supplying constraints on the spatial distribution of deformation, the forces that drive it, and the brittle and ductile properties of continental lithosphere. Deformation is usefully described as relative motions among elastic blocks and is block-like because major faults are weaker than adjacent intact crust. Despite similarities, continental block kinematics differs from global plate tectonics: blocks are much smaller, typically ~100–1000 km in size; departures from block rigidity are sometimes measurable; and blocks evolve over ~1–10 Ma timescales, particularly near their often geometrically irregular boundaries. Quantitatively relating deformation to the forces that drive it requires simplifying assumptions about the strength distribution in the lithosphere. If brittle/elastic crust is strongest, interactions among blocks control the deformation. If ductile lithosphere is the stronger, its flow properties determine the surface deformation, and a continuum approach is preferable.

## INTRODUCTION

The complexity of active continental deformation is well known and, until recently, has been difficult to quantify accurately. Complexity is evident at a broad range of scales, from a local geologic map that records evidence of past tectonism to a continent-scale seismicity map that shows a widespread distribution of earthquake epicenters. Quantifying current deformation has been difficult because no observational method was available for accurately measuring the broadly distributed and complex patterns of movement. Methods of space geodesy have now overcome this difficulty (Segall & Davis 1997, Bürgmann et al. 2000). Measurements made largely during the past decade have provided detailed mappings of present-day velocity fields across many active regions, which shed new light on how continents deform.

The velocity field for Tibet and adjacent regions (**Figure 1**) illustrates how the new deformation measurements are addressing longstanding questions about the tectonics of the India-Eurasia collision zone. Global plate reconstructions show that India has converged on Eurasia at a rate of  $\sim 35 \text{ mm year}^{-1}$  for the past  $\sim 5 \text{ Ma}$  (Royer et al. 2006), and **Figure 1** shows that this convergence occurs at the same rate today. The relative importance of shortening, crustal thickening, block rotations, and eastward extrusion of China in accommodating the India-Eurasia collision have long been contentious (e.g., England & Molnar 1997a, Tapponnier et al. 2001). Details are provided in

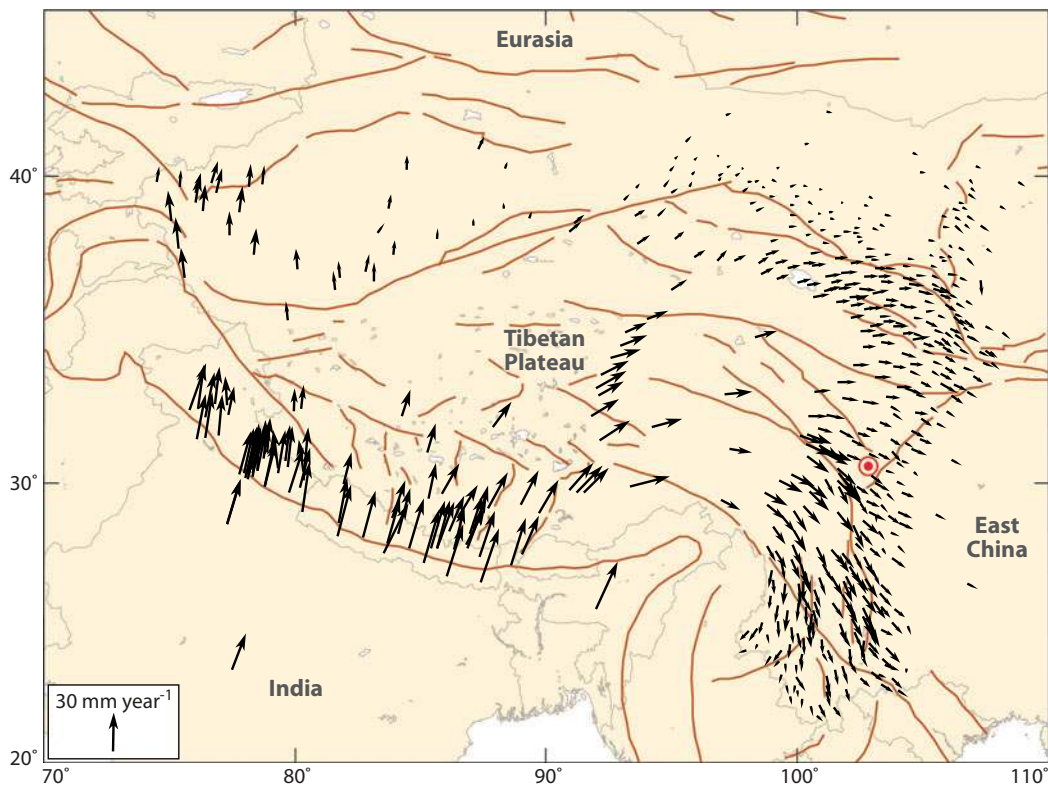


**Figure 1**

Global Positioning System (GPS) velocity field of Tibet and surrounding regions relative to Eurasia (Zhang et al. 2004). Faults are shown with faint orange lines. Bull's eye near the eastern margin of the Tibetan Plateau indicates the epicenter of the 2008 mag 7.9 Wenchuan earthquake.

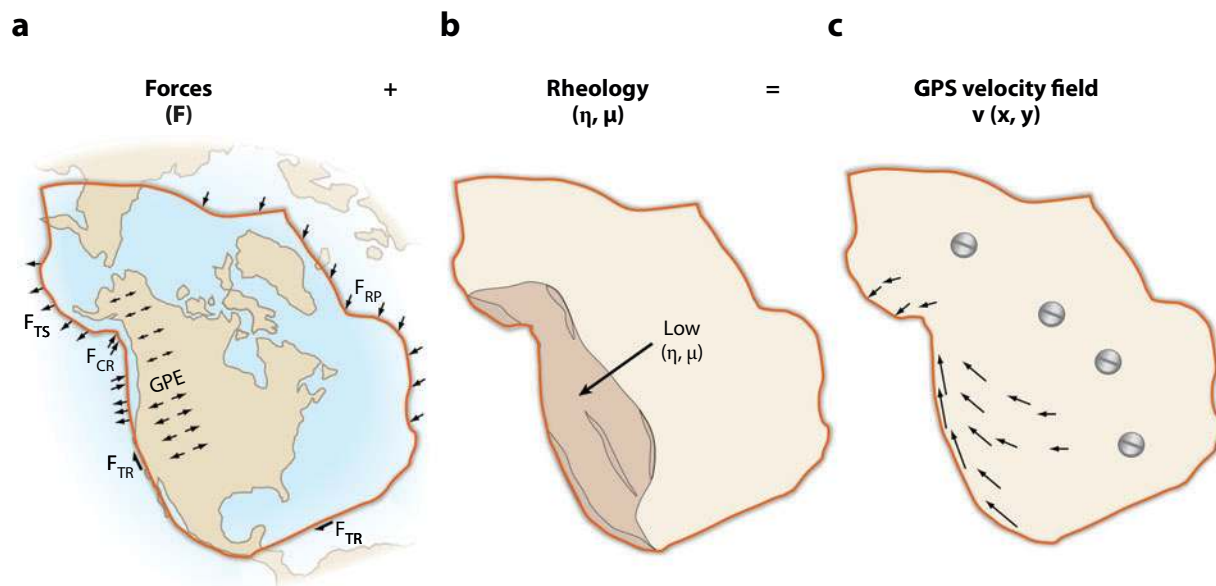


**Figure 2**

Schematic illustration showing how applied forces and lithospheric rheology determine the Global Positioning System (GPS) velocity field of the North American plate. Abbreviations: GPE, gravitational potential energy gradients;  $F_{CR}$ , collision resistance;  $F_{RP}$ , ridge push;  $F_{TR}$ , transform resistance;  $F_{TS}$ , trench suction;  $\mu$ , friction coefficient for crustal faults;  $\eta$ , viscosity of ductile lithosphere. In **Figure 2c**, arrows are GPS velocities relative to stable North America (*screwheads*). Modified from Thatcher (2003).

the Application to Active Tectonics section, but visual inspection of **Figure 1** reveals clear evidence for block rotations in several regions and no more than  $\sim 10 \text{ mm year}^{-1}$  of east-southeast motion of east China relative to Eurasia. Slip rates on the major  $\sim$ east-west-oriented strike-slip faults of Tibet have been equally controversial. As discussed later, the Global Positioning System (GPS) data indicate comparatively low current rates of 5 to  $10 \text{ mm year}^{-1}$ .

Better observational constraints on present-day movements should lead to improved process-based models of continental deformation. **Figure 2** illustrates schematically how continental deformation depends on driving forces and lithospheric strength. Forces applied to the continental lithosphere (**Figure 2a**) include the boundary forces that drive or resist plate motion that have long been known (e.g., McKenzie 1969, Forsyth & Uyeda 1975) but remain imperfectly quantified. Lateral gradients in density and thickness of the crust and the mantle lithosphere generate gradients in gravitational potential energy (GPE) (**Figure 2a**), an internal buoyancy force that can be estimated from gravity field observations and imaging of seismic velocity structure. Rheology, the rules that relate forces to deformation, determine the strength distribution within the lithosphere, due both to the material behavior of rocks (e.g., elastic, ductile) and to the shear strength of crustal faults (**Figure 2b**). Deformation, represented in **Figure 2c** as a velocity field relative to portions of currently stable continental lithosphere (screw heads in **Figure 2c**), is constrained by geologic and seismic data in addition to space geodetic observations. Simply put, **Figure 2** shows that if driving forces and rheology are specified, the distribution of deformation is determined. **Figure 2** thus represents an eminently well-posed physics problem that provides a framework for testing candidate models and constraining model parameters. Several approaches to its solution have been investigated (e.g., England & Molnar 1997b, Flesch et al. 2000), but there is still no consensus on how best to model the dynamics of continental deformation.

The main difficulty in modeling deformation is the extreme heterogeneity in spatial distribution of lithospheric strength. In the brittle/elastic upper crust, fault zones are weaker (deform at lower stresses) than the blocks they bound (e.g., Zoback et al. 1987). In the ductile lower crust and upper mantle lithosphere, strength is strongly dependent on temperature, rock type, fluid content, and stress (Kohlstedt et al. 1995). Ductile strength also depends on total strain being significantly lower in highly strained ductile shear zones than in the less deformed surrounding country rock (see Bürgmann & Dresen 2008). In the face of this complexity, two extreme end-member approaches have been applied to simplify modeling of lithospheric deformation, one emphasizing the role of the faults and discontinuous deformation in the brittle/elastic upper crust, the other focusing on the quasi-continuous straining of the ductile lithosphere (e.g., see Thatcher 1995). The block or microplate approach has been applied mainly to modeling the kinematics of deformation observed at the Earth's surface and is analogous to global plate tectonics (e.g., Avouac & Tapponnier 1993, McClusky et al. 2000). The second is a continuum fluid mechanics-based approach that unites kinematics and dynamics under the assumption that the ductile properties of the lithosphere control the deformation (see England & Jackson 1989). Which approach is better remains controversial.

The purpose of this review is to summarize results obtained from space geodetic mapping of continental deformation and to discuss their implications for active tectonics and continental dynamics. The paper is organized into six subsequent sections. The section entitled Microplate and Continuum Models evaluates the block and continuum modeling approaches based on their distinct objectives, strengths, and limitations. The sections Application to Active Tectonics and Fault Slip and Block Rotation Rates describe application of the microplate models to active tectonics, contrast continental block tectonics with global plate tectonics, and compare GPS and geologic estimates of fault slip and block rotation rates. The section Forces Driving Continental Deformation describes the forces responsible for continental deformation and uses GPS velocity field maps to illustrate the roles and local importance of particular plate boundary and internal driving forces. A summary is then followed by a short list of future research directions.

## MICROPLATE AND CONTINUUM MODELS

Although microplate and continuum models predict distinctly different deformation patterns and mechanical behavior, differences between their kinematics are ultimately gradational. Certainly, global plate tectonics, which postulates large, rigid plates and narrow bounding fault zones, differs from a continuum model with pervasive bulk deformation of a ductile material. Nonetheless, because the upper crust is brittle and elastic and because faults are weaker than the surrounding crust, deformation at the Earth's surface and through the seismogenic crust is largely block-like. However, on the actively deforming parts of continents, nominally rigid blocks are smaller and block boundary fault zones are broader than in oceanic regions. As block size decreases and the number of faults increases, the block model approaches the deformation of a continuum, and the kinematic distinction between the two models is blurred (**Figure 3**).

Therefore, in matching surface observations, the two models effectively differ only in the size and the number of blocks deemed necessary to fit the data. However, because of their distinct assumptions, each model matches observed deformation with varying degrees of success. Even when both models provide comparably good overall data fits, each will have characteristic defects. For example, continuum models must necessarily smooth through discontinuous slip across major faults and leak deformation into block interiors. In contrast, block models with a small number of elements will fail to account for intrablock deformation and mismatch data in regions containing

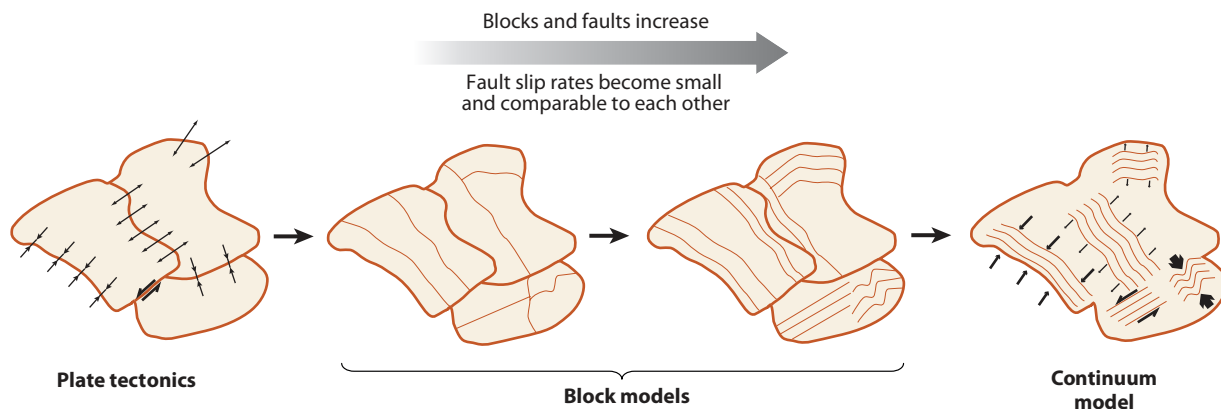


**Figure 3**

Illustration showing the transition from global plate kinematics through continental block models to continuum models. Fault slip rates become comparable to each other over the course of the transition. Bold lines denote major block boundary faults, and thin lines are faults delimiting smaller blocks. Modified from Thatcher (2007).

many small blocks. These shortcomings are not always acknowledged in published work, and evenhanded assessments of the merits of each model depend on careful evaluation of such biases and their influence on the conclusions of any study.

However, the worth of a particular model depends on more than simply a good fit to surface deformation data. Block and continuum models make different assumptions about rheology of continental lithosphere, and results are often dependent on the correctness of these idealized assumptions. Furthermore, models often have different purposes. Continuum models usually aim to address the full problem of relating driving forces to deformation (**Figure 2**). Block models have thus far been concerned only with describing the deformation of the upper crust using the methods of plate kinematics. There is thus no simple answer to the question of which model is better; in what follows, I briefly evaluate each model based on the objectives of each approach, its success in achieving these goals, and its limitations.

Continuum modeling of surface kinematics is typically a prelude to dynamic modeling of whole lithosphere deformation (e.g., England & Molnar 1997a, Flesch et al. 2000). Thus far, such models usually assume that the lithosphere is a uniform thin viscous sheet with no lateral or depth-wise variations in rheological properties. These idealizations keep the model conceptually simple and provide a computationally tractable means of quantifying the forces driving and resisting motions and relating them to observed surface deformation. An important result of these studies is the revealed importance of internal buoyancy forces in driving continental deformation (England & McKenzie 1982). Furthermore, a balance of forces analysis has permitted calculation of both internal buoyancy and plate boundary driving/resisting forces and has shown that they are often of comparable magnitude (e.g., Flesch et al. 2000). These conclusions are general because the force balance is independent of rheology for a homogeneous and isotropic material (e.g., Fung 1965) and is probably only weakly dependent on inhomogeneities in the rheology of continental lithosphere (e.g., Humphreys & Coblenz 2007). However, the next step, relating the estimated forces to deformation, is only as accurate as the approximation of lithospheric rheology. Stresses acting on a uniform thin viscous sheet produce a smoothly varying deformation field that cannot account for discontinuous fault slip or include effects due to lateral variations in ductile rheology caused by composition and thermal regime. A long-wavelength resemblance between the observed and modeled velocity fields (e.g., Flesch et al. 2001) shows a general consistency with thin viscous

sheet rheology but does not address the causes and effects of misfits to data or demonstrate that this rheology is indeed the most appropriate.

The main purpose of plate kinematic models is to quantify the rate and sense of slip across major faults and mountain belts and rotation rates of crustal blocks, with applications to active tectonics. Applications of the block model to date are restricted to matching surface kinematics, do not include any effects of the ductile lithosphere, and have not been applied to relate forces to observed deformation. However, there is no disagreement that surface deformation is largely block-like. Therefore, the utility of kinematic models depends only on how well the rotations of individual blocks are constrained and whether there is significant intrablock deformation. Both of these matters are dependent on data distribution and can be evaluated only on a case-by-case basis. In addition, the choice of blocks and block boundaries is usually subjective and sometimes in doubt, adding an additional uncertainty to model results that is difficult to quantify. Characteristic patterns of misfit residuals can be used to identify and remedy these problems, but the success of this approach again depends on data density. These issues are discussed further in connection with construction of block models and fault slip rate estimation.

Which model is most appropriate for understanding the dynamics of continental deformation (**Figure 2**) ultimately depends on lithospheric rheology, in particular whether the stresses driving continental deformation are supported predominantly in the brittle/elastic crust or in the ductile region beneath. If the ductile lithosphere is the strong element, its deformation drives the motions of a weaker, more passive upper crust and controls the kinematics of surface deformation. If high stresses are maintained in the upper crust, its block structure determines the deformation, and the weaker ductile lithosphere responds accordingly.

Constraints on lithospheric rheology are provided by laboratory rock mechanics experiments (e.g., Byerlee 1978, Kohlstedt et al. 1995), postearthquake transient deformation (Bürgmann & Dresen 2008, Thatcher & Pollitz 2008), isostatic rebound (e.g., Bills et al. 2007), and flexure due to large surface loads (e.g., Watts 2001). From this evidence, it is agreed that high lithospheric strength (deviatoric stresses  $\sim 50$ – $100$  MPa) is needed to support mountain ranges, to transmit plate boundary forces into plate interiors to drive deformation, and to store elastic strains to generate earthquakes. However, there is no consensus on the depth distribution of strength in continental lithosphere. For samples of recent opinion, see Jackson (2002), Burov & Watts (2006), and Thatcher & Pollitz (2008).

## APPLICATION TO ACTIVE TECTONICS

An important goal of active tectonics is to relate present-day instantaneous deformation reflected by crustal movements and earthquake occurrence with integrated geologic measures of recent deformation, such as faulting and block rotation. GPS velocity fields, like that shown for Tibet in **Figure 1**, contain effects of both large-scale regional deformation that can be related to active tectonics and local effects due to earthquake-cycle deformation near major faults.

### Earthquake-Cycle Deformation

Earthquake-cycle deformation, long a central focus of tectonic geodesy, is now well documented and largely understood. Both purely elastic fault models and those including the response of the ductile lithosphere predict generally similar deformation patterns at the Earth's surface (Savage 1983, 1990; Thatcher 1983; Thatcher & Rundle 1984; Tse & Rice 1986). Transient deformation following mag  $> 7$  earthquakes may persist for many decades. For studies focused on steady-state deformation, these data are either excluded or corrected for using a postseismic model. For many

velocity fields, including **Figure 1**, coseismic earthquake displacements and postseismic transient motions are absent or have been removed, and only the effect of interseismic strain accumulation need be accounted for. In the absence of large earthquakes, seismically active faults are locked (do not slip) throughout most or all of the upper crust but creep aseismically or deform by localized ductile flow at greater depths. Simple two-dimensional (2D) analysis using elastic dislocation theory (Savage 1983) shows that for faults much longer than they are wide the surface strain caused by creep beneath locked faults decreases with distance ( $x$ ) from the fault approximately as the inverse square of  $x/W$ , where  $W$  is down-dip width of the locked zone. For vertical strike-slip faults and high-angle dip-slip faults, where  $W \sim 10\text{--}20$  km, the interseismic strain becomes negligible beyond  $\sim 50\text{--}100$  km from the fault trace. For low-angle dip-slip faults with  $W \sim 100$  km or more, effects of elastic strain accumulation are important up to hundreds of kilometers from the down-dip edge of the locked fault. For nonplanar, three-dimensional (3D) fault zones, the same approximate rules apply, and complexity in fault geometry can be modeled to desired precision by tiling planar fault segments together using elementary solutions for a single rectangular fault element (Okada 1985). First-order earthquake-cycle effects can thus be removed from the observed velocity field, isolating the large-scale steady-state deformation for separate analysis and interpretation.

### Block Model Analysis

Block model analysis of velocity fields provides a simple and convenient means of extracting information such as slip rate and direction of slip across major faults and rotation rate of crustal blocks. Incorporating elastic strain accumulation into the models is conceptually straightforward (see McCaffrey 2005, Meade & Hager 2005) but complicates the analysis. In the case of Tibet, effects of interseismic deformation are unimportant for the strike-slip and normal faults of the plateau but cannot be ignored for shallow-angle thrust faults at the Himalayan front. To keep the discussion simple and illustrate general features, I exclude GPS data from the Himalayas in the following analysis and do not model effects of elastic strain accumulation. A retrospective examination of residual misfit velocities validates this approach (Thatcher 2007).

**Figure 4** illustrates how block model analysis works for the GPS velocity field of Tibet shown in **Figure 1**. First, candidate blocks are chosen based on the locations of major faults. For example, the northeast Tibet (NET) block (**Figure 4**) is bounded on the northwest by the Altyn Tagh Fault, on the north by the Qilian Shan (QS) Thrusts and the Haiyuan Fault, on the east by the Sichuan Basin, and on the south by the Qaidam Basin and the Kunlun Fault. With this block definition, all of the GPS vectors lying within the green shaded region are then used to determine the location and rotation rate for the best fitting vertical rotation axis (three model parameters, collectively termed the Euler vector; see Cox & Hart 1986). The process is then repeated for four other candidate blocks bounded by major faults, as shown in **Figure 4**. Average velocities are estimated for six other blocks containing too few precise observations to determine rotation parameters.

To assess how well the model matches the data, **Figure 4** shows small circles (circular line segments) centered on the rotation axis, labeled with the magnitude of motion relative to Eurasia (in millimeters per year) determined by the block rotation rate (e.g.,  $0.46^\circ \pm 0.02^\circ \text{ Ma}^{-1}$  for the NET block). For a perfect fit, all observed vectors would be tangent to these circular arcs, with velocity magnitude given by the indicated numbers on each arc. Visual inspection shows that the  $\sim 80^\circ$  clockwise rotation in the observed velocity vectors within the NET block agrees well with the model. Examination of misfit residuals (not shown) demonstrates their magnitudes agree correspondingly well, confirms the good fit, and determines the location of the rotation axis within a small uncertainty ( $\pm 40$  km or better). Systematic patterns in the residuals reveal defects

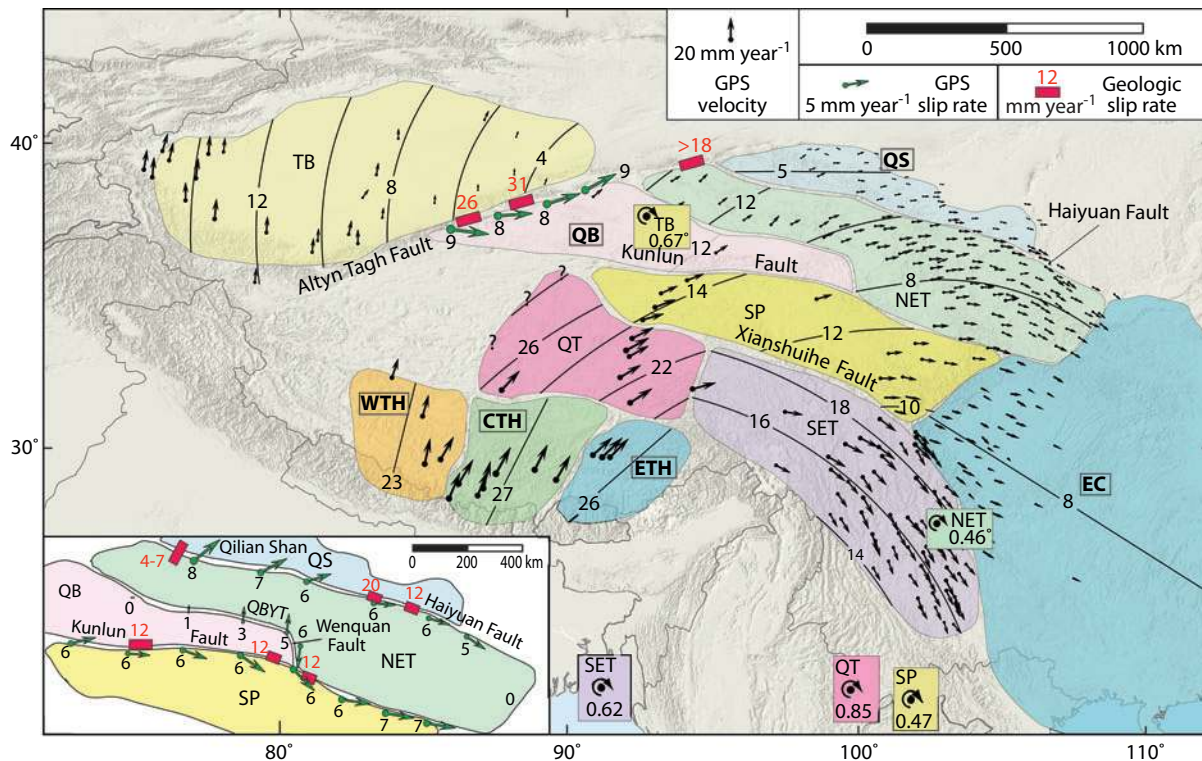


**Figure 4**

Observed Global Positioning System (GPS) velocity field of Tibet relative to Eurasia (*black arrows*), block model (*colored regions*), and some predicted interblock velocities (*green arrows*). Euler poles (rotation axes) for five blocks are color-coded to the appropriate block, with rotation rate in degree  $\text{Ma}^{-1}$ . Circular arcs show predicted velocities, with rates given in  $\text{mm year}^{-1}$ . Average translation velocities predicted for six other blocks (abbreviated names in *rectangles*) are shown as straight line segments, with rate in  $\text{mm year}^{-1}$ .

Geologically estimated slip-rate localities are indicated by red rectangles, with rates in  $\text{mm year}^{-1}$ . Inset (*lower left*) shows GPS and geologic slip-rate estimates for the NET and adjacent blocks. Block name abbreviations: NET, northeast Tibet; QT, Qiangtang; SET, southeast Tibet; SP, Songpan; TB, Tarim Basin; CTH, central Tibet Himalaya; EC, East China; ETH, eastern Tibet Himalaya; WTH, western Tibet Himalaya; QB, Qaidam Basin; QS, Qilian Shan.

in the model, which might be remedied by modifying block geometry or including unmodeled effects of elastic strain accumulation. For example, near the southwest end of the southeast Tibet (SET) block, observed vectors consistently depart  $\sim 15^\circ$  clockwise from the tangent direction of the  $16 \text{ mm year}^{-1}$  circle, indicating more complexity than is modeled using a single rigid block [see Shen et al. (2005) for a better fitting model with three additional blocks and see Meade (2007) for another block model for Tibet].

### Block Model Predictions

The model derived in this way shows a relatively simple pattern of movements. Deformation of Tibet north of the Himalayas is dominated by clockwise rotation of crustal blocks around the eastern Himalayas, accommodated largely by shear on east- and southeast-trending strike-slip faults. The majority of the deformation is thus confined in or near the Tibetan Plateau. There is only  $8 \text{ mm year}^{-1}$  of south-southeast translation of eastern China (EC) toward the trenches of southern Asia and the western Pacific.



On a more local scale, relative motions between blocks provide simple kinematic explanations for apparently complex tectonic deformation. For example, the changing styles of deformation along the boundaries of the NET block independently documented by geological studies (see Meyer et al. 1998, figure 15*a*, Wang & Burchfiel 2004, figure 2) can be understood solely by considering motion of the NET block relative to its neighbors (**Figure 4**, inset). Along its northern boundary, the geologically documented transition from nearly pure thrusting beneath the Qilian Shan Range to purely strike-slip motion across the Haiyuan Fault is clearly seen in the predicted relative motions between the NET and QS blocks, as demonstrated by the green arrows in the **Figure 4** inset. On the southeast boundary between the NET and EC blocks, little relative motion is predicted, consistent with the absence of significant geologically measured deformation. Along its southern boundary, relative motions among the NET, Qaidam Basin (QB), and Songpan (SP) blocks range from negligible in the west, to modest thrusting across the Quibeiyan Thrust (QBYT), to right-lateral strike-slip on the north-northwest/east-southeast-oriented Wenquan Fault, and to left-lateral strike-slip on the eastern Kunlun Fault. These features agree with results obtained from regional mapping of late Cenozoic deformation by Meyer et al. (1998) and Wang & Burchfiel (2004). However, there are apparently several significant differences between geologic and GPS-based fault slip rate estimates for the faults bounding the NET block, and these discrepancies are discussed later.

It is also true that block models sometimes predict fault motions that do not agree with other indicators of recent deformation. These include the northwest-trending boundary between the SP and QT blocks and the QT/SET boundary. In both localities, 10–13 mm year<sup>-1</sup> of relative motion are predicted, but active faulting and seismicity are sparse. GPS coverage here is poor, and different boundaries and/or additional blocks may be present (Meade 2007). The 2008 mag 7.9 Wenchuan earthquake (**Figure 1**, bull's eye) near the eastern margin of the Tibetan Plateau on faults with slip rates of ~1 to 3 mm year<sup>-1</sup> (Burchfiel et al. 2008) highlights the limitations of a simple block model like **Figure 4** in accounting for motions on low-slip rate faults near complex block boundaries.

## Block Models of the Western United States and the Middle East

Dense GPS networks have also been established in other regions of intracontinental deformation, and **Figures 5** and **6** show block models and representative velocity vectors for western North America (McCaffrey 2005, McCaffrey et al. 2007, McCaffrey 2008) and the Middle East (Reilinger et al. 2006). The large-scale velocity field for western North America is particularly simple, describing a roughly clockwise rotation around an axis located to the north and east of the deforming region. High velocity gradients across identified faults and rotations evident in the local velocity field constrain the block structure and smaller-scale rotations shown in **Figure 5**. In western California and northwestern Mexico, high GPS velocity gradients and active faults with slip rates of ~5 to 40 mm year<sup>-1</sup> indicate the existence of many small blocks less than ~100 km wide and often elongated approximately parallel to the direction of Pacific/North America relative plate motion (see also d'Alessio et al. 2005, Meade & Hager 2005). The velocity field for the eastern Mediterranean and the Middle East is more complex (**Figure 6**). Convergence of the Arabia and Nubia plates toward Eurasia produces generally north-directed motions north of Arabia. Northwest of Arabia, west-directed velocities take on an increasing southerly component toward the Hellenic Trench. Comparably complete GPS velocity fields and corresponding block models have been obtained in New Zealand (Wallace et al. 2004a) and central Japan (Nishimura et al. 2007).

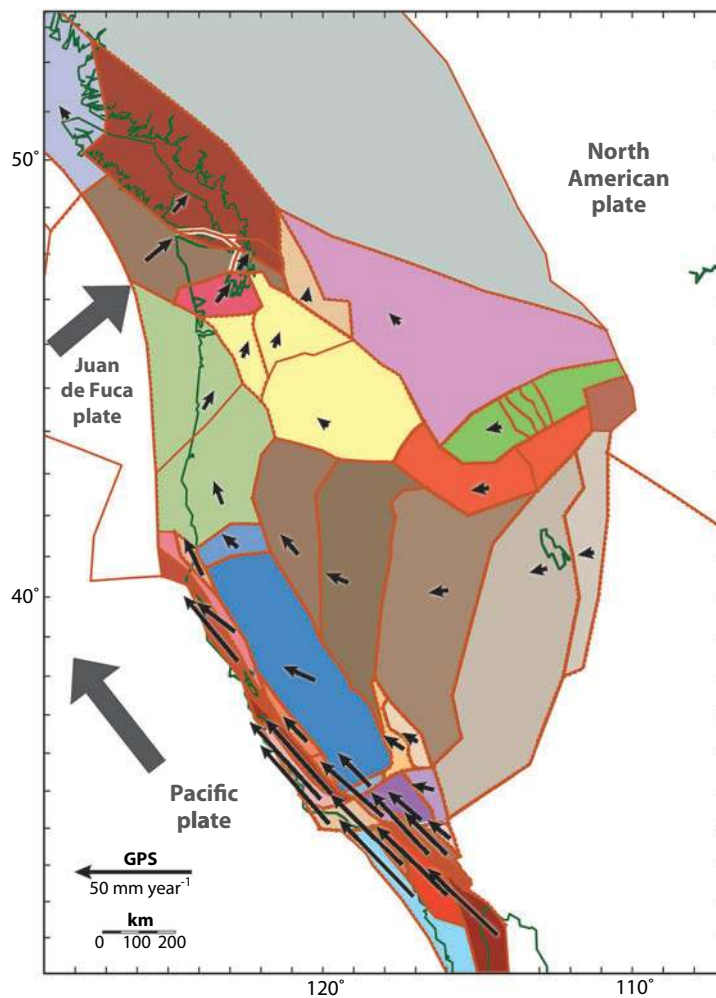


**Figure 5**

Block model of the western United States (McCaffrey 2005, McCaffrey et al. 2007, McCaffrey 2008). Large gray arrows show velocities of major plates, and small black arrows show typical velocities of continental blocks with respect to stable North America. Adjacent blocks with same or similar colors have only slightly different Euler vectors.

### Differences Between Plate Tectonics and Continental Block Tectonics

Present-day continental deformation can thus be conveniently described as relative motions among crustal blocks, using the rules of plate tectonics. However, there are several notable differences between active deformation of continents and ocean basins.

1. As **Figures 4 to 6** show, deformation is more widespread and continental blocks are typically ~100–1000 km in size, which is much smaller than major oceanic plates.
2. Many block interiors are seismically active, contain some young faults, and deform at low and sometimes detectable strain rates (Thatcher et al. 1999, Nyst & Thatcher 2004, McCaffrey 2005, Hammond & Thatcher 2005).

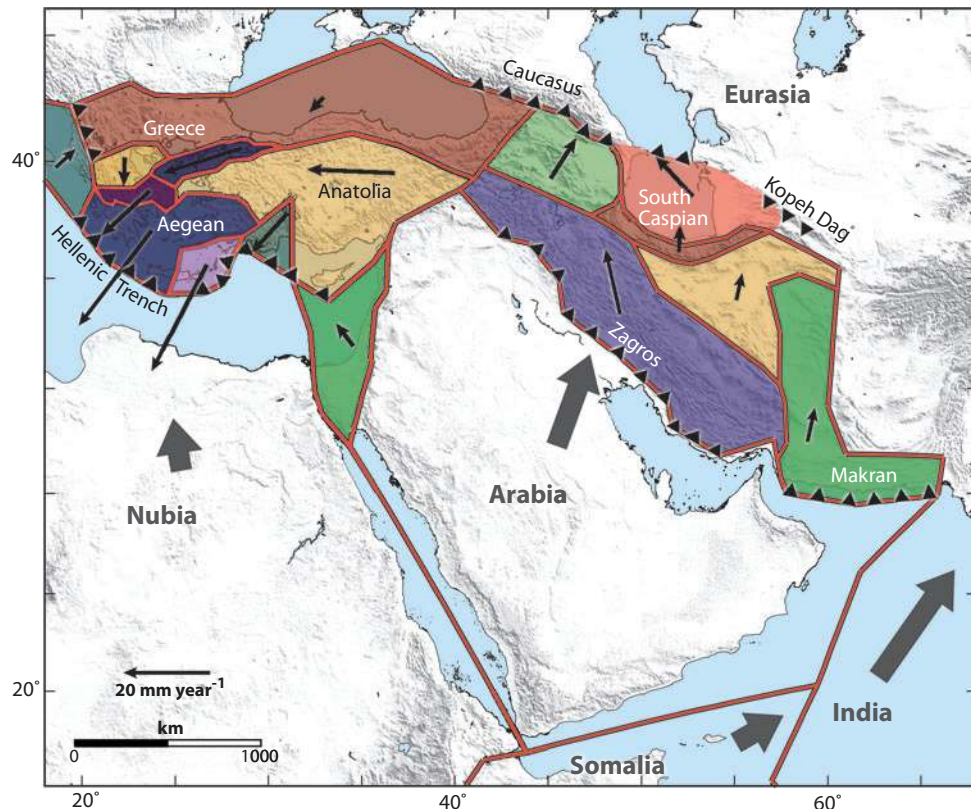


**Figure 6**

Major global plates (*bold type*) and continental blocks (*colored*) of the eastern Mediterranean and the Middle East, modified from Reilinger et al. (2006). Velocities of major plates relative to Eurasia are shown with large gray arrows. Typical velocities of smaller continental blocks, also relative to Eurasia, have thin black arrows. Solid triangles denote overthrust block at convergent boundaries.

3. In contrast to the smooth curves that mark oceanic transform and subduction plate boundaries, continental block boundaries are often irregular and complex. In part, this complexity is due to the generally small cumulative offset across continental faults. For example, strike-slip faults typically form arrays comprising discontinuous traces and numerous en echelon offsets that only become simpler when cumulative offset exceeds  $\sim 50$  km (Wesnousky 1988).
4. Furthermore, even major faults such as the San Andreas, Alpine, Altyn Tagh, and North Anatolian Faults, with cumulative offsets of  $\sim 50$  to 500 km, do not lie on the small circle that defines the relative motion between adjacent blocks. Finite block rotations thus generate internal stresses where fault trends mismatch small-circle orientation, and these stresses eventually cause formation of new fractures on more optimally oriented faults.

Consequently, block boundary zones and ultimately the blocks themselves evolve and change. Although the large global plates persist for tens or even hundreds of millions of years, there are several reasons why the longevity of continental blocks in active regions is generally much shorter, perhaps  $\sim 1$ – $10$  Ma.

First, continued slip on mis-oriented faults produces not only local realignment of minor fault splays but also local block reorganization and creation of important new faults over times as

short as a few million years. For example, geologic reconstructions of fault offsets across the San Andreas system during the past  $\sim 12$  Ma reveal many changes in the geometry and activity of the system's numerous mapped traces (Powell & Weldon 1992, Graymer et al. 2002). In particular, the subparallel San Jacinto Fault in southern California has been activated only during the past 1–2 Ma to accommodate strike-slip motions across a major compressional bend in the southern San Andreas (Sharpe 1981). Such processes may account for the narrow, elongated blocks so typical of the Pacific–North America plate boundary in western California (**Figure 5**).

Furthermore, geologically recent changes in the configuration of major plate boundaries and the forces applied there alter the stress field in adjacent plate interiors, leading to new styles of tectonic deformation and continental block geometry. For instance, the initiation of eastward motion of the Amurian plate toward the Japanese islands is the likely cause of a change from extensional to compressional tectonics that occurred in much of back-arc Japan  $\sim 2$ –4 Ma before present (BP) (Taira 2001). The change from normal oceanic plate subduction to collision of buoyant fragments of continental or oceanic lithosphere creates a strong plate boundary resisting force that transmits compressive stresses surprisingly far into the overlying continental plate. Such collisions during the past  $\sim 5$  Ma include the Izu-Bonin arc and central Honshu (Huchon & Kitazato 1984); the Yakutat terrane and eastern Alaska (Bruhn et al. 2004); and the Idria block and northwest Greece and Albania (Jackson 1994). Such collision events produce characteristic along-arc variations in driving/resisting forces and rapid block rotations that have been detected with GPS geodesy (see Wallace et al. 2005 and Forces Driving Continental Deformation, below).

## FAULT SLIP AND BLOCK ROTATION RATES

GPS estimates of rates of fault slip and block rotation are useful in several ways. First, they provide quantitative measures of regional deformation constrained by a relatively small number of parameters. Second, fault slip rates provide important inputs for earthquake hazard calculations, and rates obtained geodetically are being increasingly applied to probabilistic seismic hazard assessment (PSHA) (e.g., WGCEP 2003). Finally, decadal rate estimates can be compared with slip rates typically averaged over  $\sim 1$ –100 thousand years (Ka) determined geologically and paleomagnetic rotation rates that are integrated over timescales of  $\sim 2$  to 10 Ma. Such comparisons provide opportunities to calibrate results obtained by independent methods, to focus on eliminating systematic errors in each method, and to constrain true temporal changes in deformation rate.

### Fault Slip Rates from GPS Velocity Profiles

In regions of isolated faults or simple block structure, where GPS sites are numerous and closely spaced, velocity profiles drawn perpendicular to major faults can be a useful means of demonstrating simplicity of deformation pattern and estimating fault slip rates (e.g., Thatcher et al. 1999, Segall 2002). Using velocity profiles in this way implicitly assumes a simple translational fault model and the absence of rotation effects in the GPS data. Where data are sparse, structure is more complex, and block rotations are important, single profiles are often of limited use and may be misleading. This is particularly true in Tibet, where profiles projected perpendicular to major faults considering only fault-parallel or fault-perpendicular components of displacement show large scatter and provide only crude slip rate estimates (Zhang et al. 2004). **Figure 4** illustrates how such scatter occurs.

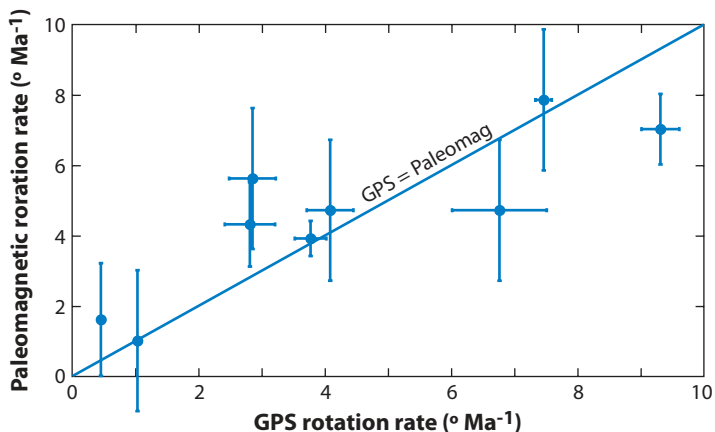


**Figure 7**

GPS versus paleomagnetic block rotation rates, with 1 SD (standard deviation) error bars as assigned by each investigator.

### Rate Comparisons


GPS and paleomagnetic block rotation rates are compared in **Figure 7** and listed in **Supplemental Table 1** (follow the **Supplemental Material link** from the Annual Reviews home page at <http://www.annualreviews.org>). GPS rates have been obtained by methods such as that illustrated for Tibet in **Figure 4** and described in section Block Model Analysis. Paleomagnetic rates for corresponding regions were derived from published determinations of magnetic declination obtained in dated rocks generally <10 Ma in age. Although only nine comparisons are available, the two independent estimates are in acceptable agreement.

There are two interrelated reasons why so few GPS/paleomagnetic comparisons are available. First, block rotation rates are generally quite small. More than half of the 60 published GPS rates (see **Supplemental Table 2**) are <1° Ma<sup>-1</sup>, and only ~10% are >3° Ma<sup>-1</sup>. Second, the typical uncertainty in paleomagnetic declination measurements is ±5°–10° (Demarest 1983), so only large rotation rates are likely to be detectable paleomagnetically. Indeed, seven of the nine comparisons shown in **Figure 7** are for rates >3° Ma<sup>-1</sup>.

GPS and geologic slip rates are compared in **Figure 8** and listed in **Supplementary Table 3**. GPS rates were obtained from relative motions between adjacent blocks, as illustrated in **Figure 4**. Geologic estimates come from measured offsets of dated geologic units or physiographic features displaced by faulting that range in age from Holocene (last 10 Ka) to late Quaternary (last 125 Ka). Although the eye is inevitably drawn to outliers, **Figure 8** shows that the majority of the GPS/geologic rate pairs agree within their nominal uncertainties (±1 standard deviation error bars taken from each published study are plotted in **Figures 7** and **8**). Among the largest mismatches are for slip rate estimates from three of the major left-lateral strike-slip faults of Tibet, where geologic rates are typically a factor of 2 to 3 larger than GPS rates (see **Figures 4** and **8**). The causes of these and other disagreements shown in **Figure 8** are unresolved and remain controversial.

### Potential Causes of Rate Discrepancies

GPS/geologic slip rate discrepancies could imply a temporal change in deformation rate, as has been suggested for several regions (e.g., Bennett et al. 2004, Chevalier et al. 2004, Oskin et al. 2008).

 **Supplemental Material**

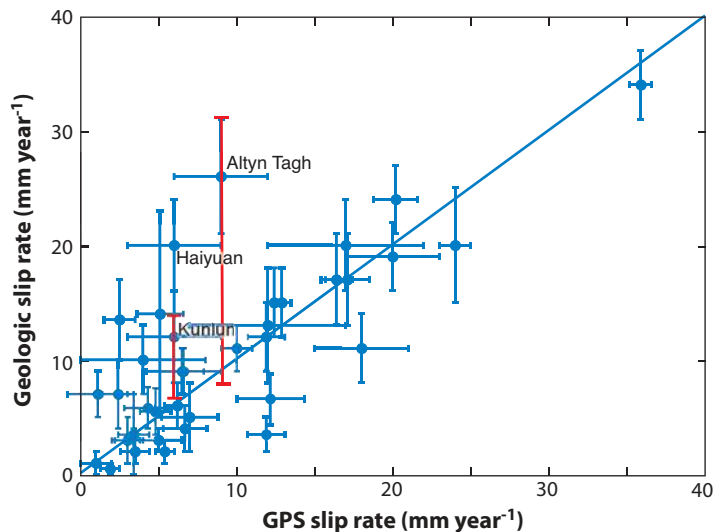


**Figure 8**

GPS versus geologic slip rates, with 1 SD (standard deviation) error bars, as assigned by each investigator. Determinations for three major strike-slip faults in Tibet are labeled as shown (see **Figure 4** for locations). Red error bars for Altn Tagh and Kunlun Faults show the larger uncertainty in geologic slip rate estimated by Cowgill (2007). All plotted values are listed in **Supplementary Table 3**.

Supplemental Material

However, a critical examination of both rate estimates is necessary to firmly establish the reliability of any suspected temporal change.

GPS slip rates are only as good as the data constraints on the block models. Model features and derived slip rates can be evaluated using several simple criteria. First, redundant observations spanning each block are needed to accurately determine rotation parameters. For example, in Tibet (**Figure 4**) the distribution and number of GPS vectors is generally good for the Tarim Basin (TB) and NET blocks but much poorer for the QB, QT, and SP blocks. Second, velocities predicted by the block rotation model should fit the data well; systematic patterns in misfit residuals indicate unmodeled complexity. Third, motions of small blocks are usually more poorly constrained than large blocks because (a) fewer data are generally available for small blocks; (b) elastic strain accumulation occurs through much or all of the block and can be difficult to separate from rotation effects; and (c) intrablock velocity gradients due to rotation are often too small to constrain rotation parameters. An additional limitation of block models, usually difficult to evaluate quantitatively, is the effect of alternative block geometries. The choice of blocks is usually to some degree subjective and depends on the distribution of major faults. Model results are also sensitive to data density within each block, which depends on the assumed distribution of blocks. As a result, the effects of block geometry depend on details that can be evaluated only on a case-by-case basis by testing plausible alternatives.

Geologic slip rate estimates also are subject to ambiguities of interpretation and uncertainties larger than their nominal error bars. A complete discussion is beyond the scope of this review, but several examples illustrate some of the important issues. For example, Cowgill (2007) has pointed out that slip rates based on offsets of fluvial terrace risers in Tibet, Turkey, and California may have large unacknowledged uncertainties because the true date of initiation of offset is bracketed only by the ages of the upper and lower terraces separated by the riser. On the Altn Tagh and Kunlun Faults in Tibet, these upper and lower terrace ages differ by factors of 2 to 3 (Hanks

& Thatcher 2006); thus, the actual uncertainties in geologic slip rates are comparably large (**Figure 8**, red error bars), and the GPS rates lie within these broad limits. It is also true that determining cumulative slip rates across complex multistranded fault zones is geologically challenging, and rates across these zones may be consistently underestimated. For example, Oskin et al. (2007) have noted that a GPS/geologic rate discrepancy across the eastern California shear zone may be due in part to distributed off-fault deformation not captured in their geologic studies.

## FORCES DRIVING CONTINENTAL DEFORMATION

### Important Forces

Continental lithosphere is deformed by the same forces that drive and resist plate motions on a global scale (**Figure 2a**). Lateral differences in crust and mantle lithosphere density and thickness generate gradients in gravitational potential energy per unit area (GPE) that are equivalent to horizontal stress gradients (e.g., England & Jackson 1989). Flow in the asthenosphere may either drive or resist motions of the overlying plates. Forces applied at plate boundaries stress the interior.  $F_{RP}$  is the familiar ridge push force due to cooling and thickening of oceanic lithosphere as it is advected away from mid-ocean ridges. Fault friction resists plate motion, producing a shear force ( $F_{TR}$ ) parallel to transform boundaries. Similar forces act on subduction and mid-ocean ridge faults, but for convenience, they are often lumped together with other forces acting at these boundaries. For example, at subduction zones, these also include forces due to (a) the negative buoyancy of the descending lithosphere (slab pull); (b) a viscous drag force resisting that descent; (c) corner flow in the asthenospheric wedge, driven by slab subduction; (d) differences between the thickness and the density distributions within continental and oceanic crust, which creates GPE gradients in the vicinity of subduction zones; (e) slab rollback, where the trench axis retreats oceanward relative to the back arc; and (f) subduction of unusually buoyant lithosphere, such as thickened ocean crust or continental lithosphere, causing collision resistance ( $F_{CR}$ ). In dynamic modeling of plate boundaries, the combined effects of these seven forces are often lumped into two equivalent forces, one trench parallel and the other trench normal (e.g., Humphreys & Coblentz 2007). A normal force directed oceanward is sometimes termed trench suction ( $F_{TS}$ ) and is implicitly associated with slab rollback. If the normal force points toward the arc, it is often called collision resistance ( $F_{CR}$ ). In what follows, I retain these terms, but in general the resultant normal force represents the superposition of several distinct loads whose magnitudes are not individually well constrained.

### Estimates of Force Magnitudes

The magnitudes of some of these driving forces can be estimated from data and models, and **Table 1** summarizes some typical results. Such forces are usefully quantified as the force per unit length of plate boundary or lithosphere column, in units of TN/m ( $10^{12}$  N m<sup>-1</sup>). The ridge push force can be estimated from thermal modeling of the cooling oceanic lithosphere (McKenzie 1969). Although its average value of  $\sim 3$  TN m<sup>-1</sup> is widely cited, variations in along-ridge sea-floor elevation and geoid height indicate significant departures from this mean. Frictional resistance to transform and subduction fault slip can be inferred by comparing observed surface heat flow with thermal models of frictionally generated heat. Such comparisons suggest resisting stresses no larger than  $\sim 20$  MPa (Lachenbruch & Sass 1980, Wang et al. 1995), corresponding to resisting forces of  $\sim 0.4$ – $1.0$  TN m<sup>-1</sup> averaged over a seismogenic zone 20–50 km wide. Modeling of crustal thickness variations has been used to estimate forces related to GPE gradients of  $1.5$  TN m<sup>-1</sup> across passive continental margins (Turcotte & Schubert 2002) and  $\sim 6$  TN m<sup>-1</sup> between the Tibetan

**Table 1** Estimates of Magnitudes of Forces Driving Deformation

| Driving Force                 | Abbreviation   | Magnitude (TN/m) | Method                           | Reference                  |
|-------------------------------|----------------|------------------|----------------------------------|----------------------------|
| Ridge push                    | $F_{RP}$ (GPE) | 1–6              | Model, geoid, ridge crest height | McKenzie (1969)            |
| Basal plate drive             | -              | 2–3              | Force balance model              | Ghosh et al. (2005)        |
| Basal plate drive             | -              | <0.3             | Force balance model              | Humphreys & Coblenz (2007) |
| Cratonic root drag            |                | 0.6              | Force balance model              | Humphreys & Coblenz (2007) |
| Transform resistance          | $F_{TR}$       | 1–2              | Force balance model              | Humphreys & Coblenz (2007) |
| Collision resistance          | $F_{CR}$       | 1–6              | Force balance model              | Humphreys & Coblenz (2007) |
| Trench suction                | $F_{TS}$       | 1–4              | Force balance model              | Humphreys & Coblenz (2007) |
| Continental margin topography | $G_{PE}$       | 1.5              | Geoid, model                     | Turcotte & Schubert (2002) |

Plateau and its surroundings (Molnar & Lyon-Caen 1988). Seismic imaging of crust and mantle lithosphere velocity structure has been applied to infer continental lithospheric density variations, from which GPE gradients can be calculated (Jones et al. 1996, Flesch et al. 2000, Zoback & Mooney 2003). However, results are only as good as the seismic coverage, the assumed relation between velocity and density, and the usually imperfect knowledge of the density distribution and thickness of the mantle lithosphere, resulting in GPE uncertainties that can approach a factor of two (Zoback & Mooney 2003).

Variations in geoid height, the equipotential surface of Earth's gravity field, reflect internal density heterogeneity and so provide information on lateral density gradients in the Earth and stress in the lithosphere. Effects depend on whether the density variations lie within the lithosphere or in the underlying mantle. Geoid height variations due to density gradients within the lithosphere are linearly proportional to GPE gradients if the lithosphere is in isostatic balance (Turcotte & Schubert 2002). Therefore, geoid gradients can be directly related to lithospheric stress gradients. Generally speaking, shorter wavelength geoid height differences reflect lithospheric density sources. This assumption can be checked by comparing geoid gradients with lithospheric GPE gradients calculated using seismic imaging results; the agreement is often good (e.g., Flesch et al. 2001). Geoid gradients across the western United States correspond to GPE differences of  $\sim 4 \text{ TN m}^{-1}$ . Sub-lithospheric density anomalies (e.g., slabs, hot spots) stress the lithosphere by coupling mantle flow to the overlying plates. Models of mantle flow are required to compute the effects of this flow on stress in the lithosphere (Steinberger et al. 2001), but the degree of coupling is uncertain and controversial (Humphreys & Coblenz 2007).

Balancing GPE gradients and boundary forces and matching interplate stress orientation data (Zoback 1992) provide estimates of driving force magnitudes at major plate boundaries (Richardson & Reding 1991, Flesch et al. 2000, Humphreys & Coblenz 2007). Force magnitudes are scaled by assuming that GPE gradients calculated from geoid or seismic data are known; thus, any GPE uncertainties will propagate into estimates of the other driving/resisting forces. The force balance calculations thus suggest frictional resisting forces of 1 to 2  $\text{TN m}^{-1}$  at transform faults, collision resistance of 2- to 6  $\text{TN m}^{-1}$ , and oceanward-directed trench normal forces as large as 4  $\text{TN m}^{-1}$  (Humphreys & Coblenz 2007). Asthenospheric flow may contribute significantly to the force balance, but estimates vary widely. Ghosh et al. (2005) suggest that a mismatch between push at the Indian ridge and GPE gradients from the Tibetan Plateau requires basal drive as large as 2  $\text{TN m}^{-1}$  under the Indian plate. Another calculation suggests driving flow is much less important for the North American plate ( $< 0.3 \text{ TN m}^{-1}$ ), and local drag by a cratonic root ( $0.6 \text{ TN m}^{-1}$ ) may be significant (Humphreys & Coblenz 2007).



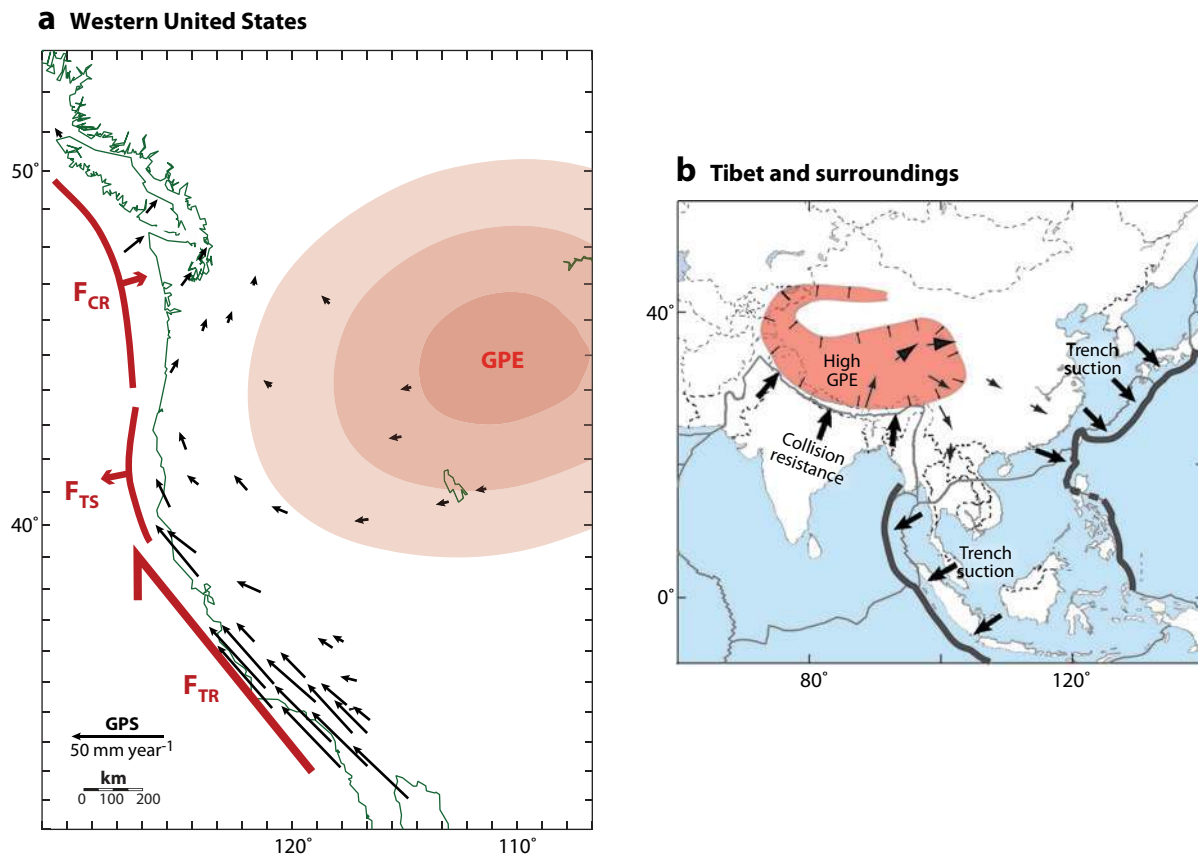


**Figure 9**  
 Forces and large-scale continental deformation. Abbreviations: GPE, gravitational potential energy gradients;  $F_{CR}$ , collision resistance;  $F_{TR}$ , transform resistance;  $F_{TS}$ , trench suction. (a) Typical western United States block velocities with respect to stable North America (arrows), plate boundary forces (red), and GPE gradient in continental lithosphere (red shading, schematic). (b) Central and eastern Asia, with plate boundary forces (bold black arrows), high GPE in Tibet (red), and representative GPS velocities relative to stable Eurasia (arrows).

## Forces and Large Scale Deformation

Driving and resisting forces stress the entire plate, but significant deformation is confined to very restricted regions. Most of the continental lithosphere is cool, thick, and strong enough to support ambient stresses without significant deformation. Active tectonic deformation is confined to regions of thermally thinned and weakened continental lithosphere, mostly in the persistently warm back arcs of current or recently active subduction zones (Hyndman et al. 2005). The GPS velocity fields in many of these deforming zones directly reflect the influence of a small number of regionally important driving forces.

In the western United States, forces applied along the Pacific–North America plate boundary are very simply related to the velocity field on the directly adjacent continental lithosphere (**Figure 9a**). Transform resistance ( $F_{TR}$ ) on the San Andreas Fault transmits boundary-parallel shear inland from the Pacific coast to western Nevada and produces elongated crustal blocks bounded by strike-slip faults (see **Figure 6**). Farther north, along the southern Cascadia subduction

zone, an outwardly directed trench suction force ( $F_{TS}$ ) generates extensional stresses oriented approximately perpendicular to the margin and GPS velocity vectors with a westward component, enhancing extensional stresses caused by GPE gradients farther inland. Finally, in northern Cascadia, some poorly understood form of subduction resistance ( $F_{CR}$ ) transmits compressional stresses inland (Humphreys & Coblenz 2007), accounting for the northeastward translation of crustal blocks in Washington and southwest Canada.

The velocity field of Tibet and its surroundings (**Figures 1 and 4**) suggests the importance of both regional and remote driving forces (**Figure 9b**). Collision resistance due to subduction of buoyant continental lithosphere at the Himalayan front transmits compressive stresses northward into central Asia. However,  $\sim 40$  Ma of continental collision has produced the high topography, thickened crust, and high GPE of the Tibetan Plateau, generating extensional stresses on the plateau and compression at its edges. On the plateau, these stresses in part counteract the collision-related compression, resulting in mixed normal and strike-slip faulting (e.g., Flesch et al. 2001). Collision resistance and GPE alone cannot explain the clockwise rotation of crustal blocks around the eastern Himalayas or the east-southeast translation of EC (**Figure 4**), which appear to require southwest-directed trench suction at the Andaman-Sumatra arc and southeast-oriented suction at the subduction zones of the western Pacific (**Figure 9b**).

The deformation of the Middle East (**Figure 6**) is largely due to the collision of Arabia with Eurasia and suction due to the rollback of the Hellenic Trench (McKenzie 1978, Le Pichon 1983, Reilinger et al. 2006). Collision resistance at the northeastern boundary of the Arabian plate produces the Zagros mountains and the Makran accretionary complex and transmits compressive stresses farther north to build the Caucasus, Alborz, and Koppeh Dag Ranges. Although slab rollback at the Hellenic Trench is a major driving force, the GPE gradient between the Anatolian Plateau and the trench generates extensional stresses that may be comparably important. The combined effects of collision resistance, trench suction, and GPE are thus very similar to those shown for Tibet and its surroundings in **Figure 9a**. However, the Middle East velocity field shows additional complexity, for example, near the Caspian Sea and in central Greece, that may be due to large locally important forces that I discuss in the next section.

### Local Forces and Block Rotation

Just as collision resistance and trench suction are important driving forces on a continental scale, they also act locally to produce characteristic tectonic features that are reflected in the GPS velocity field. Wallace et al. (2005) have shown that, in five regions of the western Pacific, the close juxtaposition of these two forces produces a locally strong torque and rapid rotation of small blocks around a nearby axis. **Figure 10** shows examples of this process acting in a number of different tectonic settings. In most of these cases, collision produces elevated regions and a GPE gradient directed toward the trench that complements the effects of the collision/suction force couple.

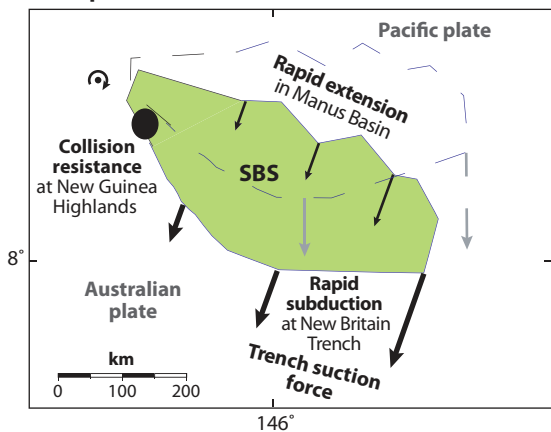
Interaction between the Australian and Pacific plates causes local continental collision at the New Guinea Highlands and subduction at the New Britain Trench. **Figure 10a** shows that this abrupt along-strike change in driving forces has produced rotation of the South Bismarck Sea

---

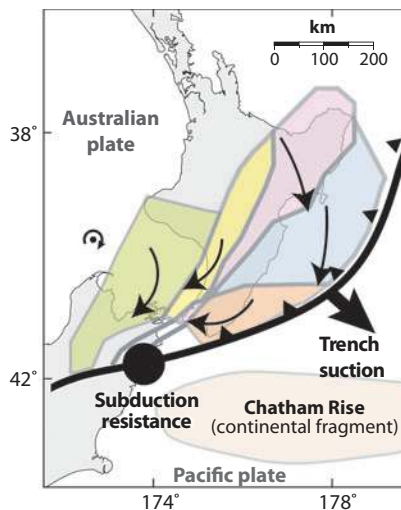
**Figure 10**

Local forces and block rotations. Subduction resistance is denoted by solid circles, trench suction by straight solid arrows, sense of block rotations by curved arrows, and rotation axes by a dot and a semicircular arrow. See text for discussion.

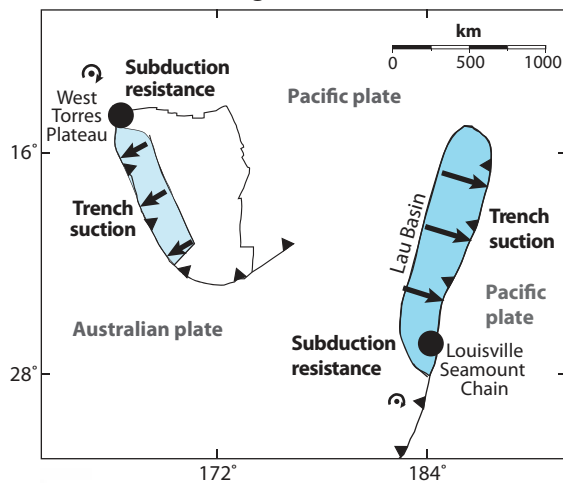
**a Papua New Guinea**



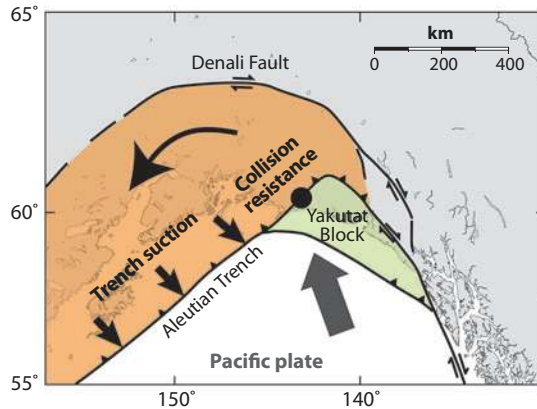
**b New Zealand**



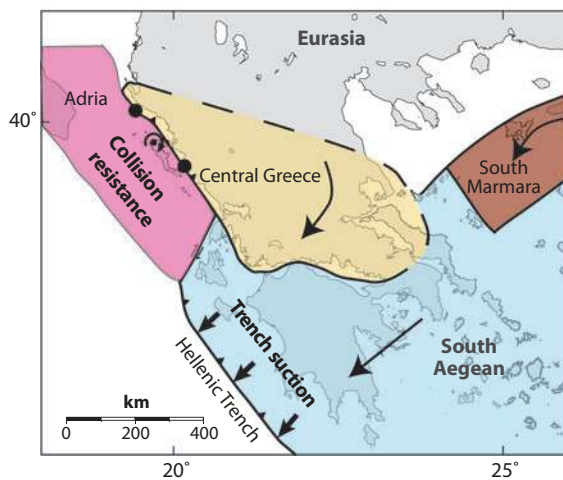
**c Vanuatu and Tonga**



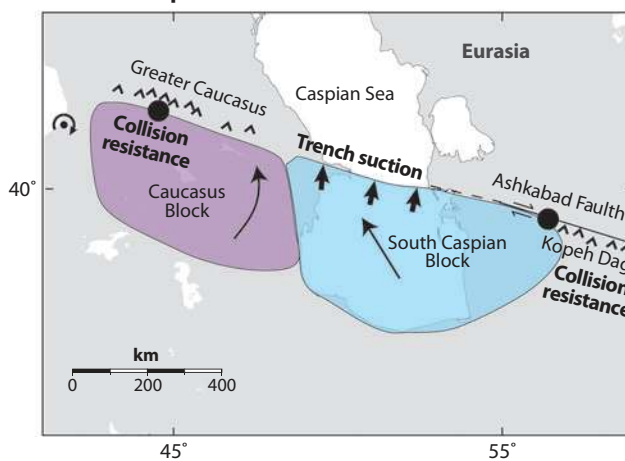
**d SE Alaska**



**e Central Greece**



**f South Caspian**



(SBS) block around an axis located near the collision zone. The clockwise (CW) rotation rate of the SBS block relative to the Australian plate constrained by GPS data is  $7.45^\circ \text{ Ma}^{-1}$  (Wallace et al. 2004b).

Suction forces at the Hikurangi Trench off eastern North Island, New Zealand and resistance to subduction of the Chatham Rise off northern South Island cause a CW torque and a rotation of five distinct crustal blocks (**Figure 10b**). Their rotation axes relative to the Australian plate are all near the single representative axis plotted in **Figure 10b**. Rotation rates range from  $0.4$  to  $3.8^\circ \text{ Ma}^{-1}$  (CW), and differential motions between the blocks causes strike-slip and reverse faulting on southern North Island and rapid extension to the north (Wallace et al. 2004a).

Forced subduction of buoyant portions of oceanic lithosphere produces effects very similar to those described above. Wallace et al. (2005) have shown that subduction of the West Torres Plateau in northern Vanuatu and normal subduction to the south causes CW rotation of two back-arc crustal slivers at  $5.9$  to  $7.6^\circ \text{ Ma}^{-1}$  relative to the Pacific plate and rapid extension in the Erromanga-Futuna Trough (**Figure 10c, left**). An analogous effect occurs in the Tonga Arc and Lau Basin due to subduction of the Louisville Seamounts (**Figure 10c, right**) and Wallace et al. (2005) suggest that this process plays an important role in back-arc rifting.

Convergence between the Yakutat terrane and the Aleutian Trench results in a small-scale continental collision in the eastern Gulf of Alaska (Bruhn et al. 2004) (**Figure 10d**). The setting has several similarities with the India/Eurasia collision and the forces acting there. In Alaska, collision produces the high mountains of the Chugach-St. Elias Range, transmits compressive stresses as much as  $\sim 1000$  km inland, and may be responsible for the counterclockwise (CCW) rotation of the Aleutian forearc (Leonard et al. 2007). **Figure 10d** shows that the collision/trench suction force couple acts in this region and provides a simple mechanism that may explain the forearc rotation.

In central Greece, GPS data document  $4.3^\circ \text{ Ma}^{-1}$  CW rotation of a crustal block lying between stable Eurasia and the Aegean Sea (Nyst & Thatcher 2004) (**Figure 10e**). The tectonic setting again suggests the action of a collision/suction force couple. The axis of rotation of the central Greece block relative to Eurasia lies close to a zone where the Apulia block is colliding with northwestern Greece and Albania. This block is pinned by collision on its western boundary and rotates CW as it is entrained in the motion of the much larger South Aegean block, which is pulled southwest by suction at the Hellenic Trench.

The South Caspian Basin is probably underlain by a remnant piece of oceanic lithosphere isolated during the Arabia/Eurasia collision that is now being subducted to the north beneath stable Eurasia (Jackson et al. 2002) (**Figure 10f**). The South Caspian Basin is bounded to the east and the west by compressive mountain belts that resist convergence (**Figure 10f**), so the subducting slab beneath the basin is likely to be retreating relative to Eurasia. GPS data demonstrate that the Caucasus block is rotating CCW around an axis at its western end (Reilinger et al. 2006), suggesting the effects of collision resistance at the Greater Caucasus and trench suction in the Caspian Basin. Fault patterns and earthquake focal mechanism data imply the South Caspian block is moving northwest or north-northwest relative to Eurasia (Jackson et al. 2002). The geometry of the South Caspian block is poorly known, its subaerial extent could be more limited than is shown in **Figure 10f**, and no GPS data are yet available to quantitatively constrain its relative motion. However, its tectonic setting suggests CW block rotation in response to a suction force on its northern boundary and collision resistance near its eastern end. Note that in this interpretation trench suction is assumed to act on the underthrust (South Caspian) block as well as on the overthrust Eurasian lithosphere to the north.

## SUMMARY POINTS

1. Space geodetic methods permit detailed strain mapping of continental lithosphere that is warm, thin, and weak enough to deform significantly (**Figures 1 and 2c**). The style of deformation (extensional, compressional, strike-slip) depends on the forces applied at the boundaries and within each active region (**Figure 2a**). Its detailed spatial distribution is controlled by lithospheric rheology (**Figure 2b**), in particular the strength of faults and intervening crustal blocks and the coupling of these blocks to the ductile lithosphere.
2. Tectonic deformation at the Earth's surface reflects the relative motions of fault-bounded blocks that extend at least through the upper crust. Deeper motions are accommodated by ductile flow. If the brittle/elastic crust is the mechanically strongest part of the lithosphere, then interactions among blocks largely determine the kinematics and dynamics of the deformation. If the ductile lithosphere is strongest, then its flow properties control the deformation. There has been longstanding disagreement on where lithospheric strength resides, leading to contrasting descriptions of continental deformation (**Figure 3**). My own view (Thatcher & Pollitz 2008) and that of others before me (e.g., Lachenbruch & Sass 1980, Townend & Zoback 2000, Jackson 2002) is that the upper crust is the predominant load-bearing element in deforming regions. But dissent remains strong (e.g., England & Molnar 1997b, Flesch et al. 2000, Burov & Watts 2006), and it is not yet agreed which rheological description best links the kinematics of deformation to the forces that drive it.
3. The GPS velocity field is a superposition of the motions of crustal blocks and cyclic buildup and release of elastic strain near major faults. Because the earthquake deformation cycle is largely understood, its first-order effects may be removed from the data, leaving only the motions of the blocks. Block models fit to GPS velocity fields are thus useful for determining slip rates on faults and rotation rates of crustal blocks. Simple models with a relatively small number of blocks can explain major features (**Figures 4, 5, and 6**), but more complex models with many blocks may well be needed to match details and determine displacement rates across low slip rate faults.
4. General agreement between GPS and geologic slip rates is encouraging (**Figure 8**). Discrepancies may represent true temporal rate changes, but both GPS and geologic estimation methods have systematic uncertainties, so disagreements must be assessed on a case-by-case basis.
5. Despite the successes of plate kinematics in matching the present-day deformation field measured by space geodesy, continental block tectonics differs in notable ways from global plate tectonics. Blocks within deforming zones on the continents are much smaller than the global plates, their interiors often contain minor active faults, and their boundaries are irregular. Finite rotations of these irregularly shaped blocks produce local stress concentrations, evolution of boundary fault zones, and eventual changes in block geometry. Block reorganization also occurs if boundary forces change, such as when buoyant oceanic or continental lithosphere collides at a trench and alters the back-arc stress field.

6. Forces driving deformation are becoming better understood and quantified. Important forces range in magnitude from  $\sim 1$  to  $6 \text{ TN m}^{-1}$  (**Table 1**), but individual values may be uncertain by a factor of two and change significantly along plate boundaries and within deforming regions. Patterns in the observed GPS velocity field often directly reflect along-boundary changes in the type of driving force (**Figures 9** and **10**). The interplay among collision resistance, high topographic gradients generated by collision (GPE), and trench suction produce particularly characteristic patterns of deformation that occur at length scales ranging from continental (**Figure 9b**) to local (**Figure 10**).

### FUTURE ISSUES

1. Despite the greatly expanded use of GPS methods during the past decade, many active regions have incomplete coverage and remain imperfectly understood (e.g., Tibetan Plateau, **Figure 1**). New GPS networks will gradually alleviate this deficiency. However, many deforming regions are vast and/or largely inaccessible and so are likely to remain sparsely covered with GPS sites. Interferometric synthetic aperture radar (InSAR) satellite imaging of surface deformation (Bürgmann et al. 2000) is a promising remote sensing method likely to improve its resolution and global coverage during the next decade, and I expect it will provide the best new deformation maps.
2. Dynamical models of continental deformation do not explicitly include faults or account for horizontal and vertical variations in rheology. New models that incorporate these effects and match GPS data should provide improved rheological constraints and better quantify the forces that drive the deformation.
3. Fault slip rates are important input to PSHA, but GPS results are only beginning to be incorporated into these calculations (e.g., WGCEP 2003). GPS slip rates should be carefully evaluated for inclusion in PSHA models, and discrepancies between geologic and GPS estimates of fault slip rates need to be critically assessed to determine the true significance of the disagreement.

### DISCLOSURE STATEMENT

The authors are not aware of any biases that might be perceived as affecting the objectivity of this review.

### ACKNOWLEDGMENTS

R. McCaffrey, R. Reilinger, and L. Wallace supplied original figures from their papers, from which **Figures 5, 6, and 10a–c** were drafted. Careful and constructive reviews were provided by R. Bürgmann, G. Fuis, T. Hanks, P. McCrory, and F. Pollitz.

### LITERATURE CITED

Avouac JP, Tapponnier P. 1993. Kinematic model of active deformation in central Asia. *Geophys. Res. Lett.* 20:895–98

- Bennett RA, Friedrich AM, Furlong KP. 2004. Co-dependent histories of the San Andreas and San Jacinto fault zones from inversion of geologic displacement rate data. *Geology* 32:961–64
- Bills BG, Adams KD, Wesnousky SG. 2007. Viscosity structure of the crust and upper mantle in western Nevada from isostatic rebound patterns of the late Peistocene Lake Lahontan high shorelines. *J. Geophys. Res.* 112:B06405
- Bruhn RL, Pavlis TL, Plafker G, Serpa L. 2004. Deformation during terrane accretion in the Saint Elias orogen, Alaska. *Geol. Soc. Am. Bull.* 116:771–87
- Burchfiel BC, Royden LH, van Der Hilst RD, Hager BH, Chen Z, et al. 2008. A geological and geophysical context for the Wenchuan earthquake of 12 May 2008, Sichuan, People's Republic of China. *GSA Today* 18:4–11
- Bürgmann R, Dresen G. 2008. Rheology of the lower crust and upper mantle: evidence from rock mechanics, geodesy, and field observations. *Annu. Rev. Earth Planet. Sci.* 36:531–67
- Bürgmann R, Rosen PA, Fielding EJ. 2000. Synthetic aperture radar interferometry to measure Earth's surface topography and its deformation. *Annu. Rev. Earth Planet. Sci.* 28:169–209
- Burov EB, Watts AB. 2006. The long-term strength of continental lithosphere: “jelly sandwich” or “creme brûlée”? *GSA Today* 12:4–10
- Byerlee J. 1978. Friction of rocks. *Pure Appl. Geophys.* 116:615–26
- Chevalier ML, Ryerson FJ, Tapponnier P, Finkel RC, Van Der Woerd J, et al. 2004. Slip-rate measurements on the Karakoram fault may imply secular variations in fault motion. *Science* 307:411–14
- Cowgill E. 2007. Impact of riser reconstructions on estimation of secular variation in rates of strike-slip faulting: revisiting the Cherchen River site along the Altyn Tagh fault, NW China. *Earth Planet. Sci. Lett.* 254:239–55
- Cox A, Hart BH. 1986. *Plate Tectonics: How It Works*. Palo Alto, CA: Blackwell. 392 pp.
- d'Alessio MA, Johansen IA, Bürgmann R, Schmidt DA, Murray MH. 2005. Slicing up the San Francisco Bay Area: block kinematics and fault slip rates from GPS-derived surface velocities. *J. Geophys. Res.* 110:BO6403
- Demarest H. 1983. Error analysis for the determination of tectonic rotation from paleomagnetic data. *J. Geophys. Res.* 88:4321–28
- England P, Molnar P. 1997a. The field of crustal velocity in Asia calculated from Quaternary rates of slip on faults. *Geophys. J. Int.* 130:551–82
- England P, Molnar P. 1997b. Active deformation of Asia: from kinematics to dynamics. *Science* 278: 647–50
- England PC, Jackson JA. 1989. Active deformation of the continents. *Annu. Rev. Earth Planet. Sci.* 17:197–226
- England PC, McKenzie DP. 1982. A thin viscous sheet model for continental deformation. *Geophys. J. R. Astron. Soc.* 70:295–321
- Flesch LM, Haines AJ, Holt WE. 2001. Dynamics of the India-Eurasia collision. *J. Geophys. Res.* 106:16435–60
- Flesch LM, Holt WE, Haines AJ, Shen-Tu B. 2000. Dynamics of the Pacific-North American plate boundary in the western United States. *Science* 287:834–36
- Forsyth D, Uyeda S. 1975. On the relative importance of the driving forces of plate motion. *Geophys. J. R. Astron. Soc.* 43:163–200
- Fung YC. 1965. *Foundations of Solid Mechanics*. Englewood Cliffs, NJ: Prentice Hall
- Ghosh A, Holt WE, Flesch LM, Haines AJ. 2005. Gravitational potential energy of the Tibetan Plateau and the forces driving the Indian plate. *Geology* 34:321–24
- Graymer RW, Sarna-Wojcicki AM, Walker JP, McLaughlin RJ, Fleck RJ. 2002. Controls on timing and amount of right-lateral offset on the East Bay fault system, San Francisco Bay region, California. *Bull. Geol. Soc. Am.* 114:1471–79
- Hammond WC, Thatcher W. 2005. Northwest basin and range tectonic deformation observed with the global positioning system, 1999–2003. *J. Geophys. Res.* 110:B10405
- Hanks TC, Thatcher W. 2006. *The slip-rate discrepancy for the Altyn Tagh Fault: an example of epistemic uncertainty*. Presented at Fall Meet. Am. Geophys. Union, San Francisco (Abstr.)
- Huchon P, Kitazato H. 1984. Collision of the Izu block with central Japan during the Quaternary and geological evolution of the Ashigara area. *Tectonophysics* 110:201–10
- Humphreys ED, Coblenz DD. 2007. North American dynamics and western U.S. tectonics. *Revs. Geophys.* 45:RG3001

- Hyndman RD, Currie CA, Mazzotti SP. 2005. Subduction zone backarcs, mobile belts, and orogenic heat. *GSA Today* 15:4–10
- Jackson J. 2002. Strength of the continental lithosphere: Time to abandon the jelly sandwich? *GSA Today* 12:4–9
- Jackson JA. 1994. Active tectonics of the Aegean region. *Annu. Rev. Earth Planet. Sci.* 22:239–71
- Jackson JA, Priestley K, Allen M, Berberian M. 2002. Active tectonics of the South Caspian Basin. *Geophys. J. Int.* 148:214–45
- Jones CH, Unruh JR, Sonder LJ. 1996. The role of gravitational potential energy in the active deformation of the southwestern United States. *Nature* 381:37–41
- Kohlstedt DL, Evans B, Mackwell SJ. 1995. Rheology of the lithosphere: constraints imposed by laboratory experiments. *J. Geophys. Res.* 100:17587–602
- Lachenbruch AH, Sass J. 1980. Heat flux and energetics of the San Andreas fault zone. *J. Geophys. Res.* 85:6185–223
- Leonard LJ, Hyndman RD, Mazzotti S, Nikolaishen L, Schmidt M, Hippchen S. 2007. Current deformation in the northern Canadian Cordillera inferred from GPS measurements. *J. Geophys. Res.* 112:B11401
- Le Pichon X. 1983. Land-locked ocean basins and continental collision: the eastern Mediterranean as a case example. In *Mountain Building Processes*, ed. KJ Hsu, pp. 201–13. London: Academic
- McCaffrey R. 2005. Block kinematics of the Pacific-North America plate boundary in the southwestern United States from inversion of GPS, seismologic and geologic data. *J. Geophys. Res.* 110:B07401
- McCaffrey R. 2008. *Estimates of permanent strain rates in the western U.S.* Presented at Annu. Meet. Geol. Soc. Am., Houston
- McCaffrey R, Qamar AI, King RW, Wells R, Khazaradze G, et al. 2007. Fault locking, block rotation and crustal deformation in the Pacific Northwest. *Geophys. J. Int.* 169:1315–40
- McClusky S, Balassanian S, Barka A, Demir C, Ergintav S, et al. 2000. Global Positioning System constraints on plate kinematics and dynamics in the eastern Mediterranean and Caucasus. *J. Geophys. Res.* 105:5695–719
- McKenzie DP. 1969. Speculations on the consequences and causes of plate motions. *Geophys. J. R. Astron. Soc.* 18:1–32
- McKenzie DP. 1978. Active tectonics of the Alpine Himalayan Belt, the Aegean Sea and surrounding regions. *Geophys. J. R. Astron. Soc.* 55:217–52
- Meade BJ. 2007. Present-day kinematics at the India-Asia collision zone. *Geology* 35:81–84
- Meade BJ, Hager BH. 2005. Block models of crustal motion in southern California constrained by GPS measurements. *J. Geophys. Res.* 110:B03403
- Meyer B, Tapponnier P, Bourjot L, Metivier F, Gaudemer Y, et al. 1998. Crustal thickening in Gansu-Xinghai, lithospheric mantle subduction, and oblique, strike-slip controlled growth of the Tibetan plateau. *Geophys. J. Int.* 135:1–47
- Molnar P, Lyon-Caen H. 1988. Some simple physical aspects of the support, structure, and evolution of mountain belts. In *Processes in Continental Deformation*, ed. SP Clark, BC Burchfiel, J Suppe. *Geol. Soc. Am. Spec. Pap.* 218:179–207
- Nishimura T, Sagiya T, Stein RS. 2007. Crustal block kinematics and seismic potential of the northernmost Philippine Sea plate and Izu microplate, central Japan, inferred from GPS and leveling data. *J. Geophys. Res.* 112:B05414
- Nyst M, Thatcher W. 2004. New constraints on the active tectonic deformation of the Aegean. *J. Geophys. Res.* 109:B11406
- Okada Y. 1985. Surface deformation due to shear and tensile faults in a half-space. *Bull. Seismol. Soc. Am.* 75:1135–54
- Oskin M, Perg L, Blumentritt D, Mukhopadhyay S, Iriondo A. 2007. Slip rate of the Calico fault: implications for geologic versus geodetic rate discrepancy in the eastern California shear zone. *J. Geophys. Res.* 112:B03402
- Oskin M, Perg L, Shelef E, Gurney E, Singer B, Zhang X. 2008. Elevated shear zone loading rate during an earthquake cluster in eastern California. *Geology* 36:507–10
- Powell RE, Weldon RJ. 1992. Evolution of the San Andreas Fault. *Annu. Rev. Earth Planet. Sci.* 20:431–68



- Reilinger R, McClusky S, Vernant P, Lawrence S, Ergintav S, et al. 2006. GPS constraints on continental deformation in the Africa-Arabia-Eurasia continental collision zone and implications for the dynamics of plate interactions. *J. Geophys. Res.* 111:B05411
- Richardson RM, Reding LM. 1991. North American plate dynamics. *J. Geophys. Res.* 96:12201–23
- Royer JY, Gordon RG, Horner-Johnson BC. 2006. Motion of Nubia relative to Antarctica since 11 Ma: Implications for Nubia-Somalia, Pacific–North America, and India-Eurasia motion. *Geology* 34:501–4
- Savage JC. 1983. Strain accumulation in western United States. *Annu. Rev. Earth Planet. Sci.* 11:11–43
- Savage JC. 1990. Equivalent strike-slip earthquake cycles in half-space and lithosphere-asthenosphere earth models. *J. Geophys. Res.* 95:4873–79
- Segall P. 2002. Integrating geologic and geodetic estimates of slip rate on the San Andreas Fault System. *Int. Geol. Rev.* 44:62–82
- Segall P, Davis JL. 1997. GPS applications for geodynamics and earthquake studies. *Annu. Rev. Earth Planet. Sci.* 23:301–36
- Sharpe RV. 1981. Variable rates of late Quaternary strike-slip on the San Jacinto fault zone, southern California. *J. Geophys. Res.* 86:1754–62
- Shen ZK, Lu J, Wang M, Burgmann R. 2005. Contemporary crustal deformation around the southeast borderland of the Tibetan Plateau. *J. Geophys. Res.* 110:B003421
- Smith DA, Roman DR. 2001. GEOID99 and G99SSS: 1-arc minute geoid models for the United States. *J. Geodesy* 75:469–90
- Steinberger B, Schmelting H, Marquart G. 2001. Large-scale lithospheric stress field and topography induced by global mantle circulation. *Earth Planet. Sci. Lett.* 186:75–91
- Taira A. 2001. Tectonic evolution of the Japanese Island arc system. *Annu. Rev. Earth Planet. Sci.* 29:109–34
- Tapponnier P, Xu Z, Roger F, Meyer B, Arnaud N, et al. 2001. Oblique step-wise growth of the Tibetan Plateau. *Science* 294:1671–77
- Thatcher W. 1983. Nonlinear strain buildup and the earthquake deformation cycle on the San Andreas fault. *J. Geophys. Res.* 88:5893–902
- Thatcher W. 1995. Continuum versus microplate models of active continental deformation. *J. Geophys. Res.* 100:3885–94
- Thatcher W. 2003. GPS constraints on the kinematics of continental deformation. *Int. Geol. Rev.* 45:191–212
- Thatcher W. 2007. Microplate model for the present-day deformation of Tibet. *J. Geophys. Res.* 112:B01401
- Thatcher W, Foulger GR, Julian BR, Svarc J, Quilty E, Bawden GW. 1999. Present day deformation across the basin and range province, western United States. *Science* 283:1714–18
- Thatcher W, Pollitz F. 2008. Temporal evolution of continental lithospheric strength in actively deforming regions. *GSA Today* 18:4–11
- Thatcher W, Rundle JB. 1984. A viscoelastic coupling model for the cyclic deformation due to periodically repeated earthquakes at subduction zones. *J. Geophys. Res.* 89:7631–40
- Townend J, Zoback ML. 2000. How faulting keeps the crust strong. *Geology* 28:399–402
- Tse ST, Rice JR. 1986. Crustal earthquake instability in relation to the depth variation of frictional slip properties. *J. Geophys. Res.* 91:9452–72
- Turcotte DL, Schubert G. 2002. *Geodynamics*. Cambridge, UK: Cambridge Univ. Press. 2nd ed.
- Wallace LM, Beavan J, McCaffrey R, Darby D. 2004a. Subduction zone coupling and tectonic block rotations in the North Island, New Zealand. *J. Geophys. Res.* 109:B12406
- Wallace LM, McCaffrey R, Beavan J, Ellis S. 2005. Rapid microplate rotations and backarc rifting at the transition between collision and subduction. *Geology* 33:857–60
- Wallace LM, Stevens CW, Silver E, McCaffrey R, Lorantung W, et al. 2004b. GPS constraints on active tectonics and arc-continent collision in Papua New Guinea: evidence for edge-driven microplate rotations. *J. Geophys. Res.* 109:B05404
- Wang E, Burchfiel BC. 2004. Late Cenozoic right-lateral movement along the Wenquan fault and associated deformation: implications for the kinematic history of the Qaidam basin, northeastern Tibetan Plateau. *Int. Geol. Rev.* 46:861–79
- Wang K, Mulder T, Rogers GC, Hyndman RD. 1995. Case for very low coupling stress on the Cascadia subduction fault. *J. Geophys. Res.* 100:12907–18

- Watts AG. 2001. *Isostasy and Flexure of the Lithosphere*. Cambridge, NY: Cambridge Univ. Press
- Wesnousky SG. 1988. Seismological and structural evolution of strike-slip faults. *Nature* 335:340–42
- Work. Group Calif. Earthq. Probab. (WGCEP). 2003. Earthquake probabilities in the San Francisco Bay region: 2002–2031. *U. S. Geol. Surv. Open File Rep.* 03–214
- Zhang P-Z, Shen Z, Wang M, Gan W, Burgmann R, et al. 2004. Continuous deformation of the Tibetan Plateau from global positioning system data. *Geology* 32:809–12
- Zoback MD, Zoback ML, Mount VS, Suppe J, Eaton JP, et al. 1987. New evidence on the state of stress of the San Andreas fault system. *Science* 238:1105–11
- Zoback ML. 1992. First- and second-order patterns of stress in the lithosphere: the World Stress Map Project. *J. Geophys. Res.* 97:11702–28
- Zoback ML, Mooney WD. 2003. Lithospheric buoyancy and continental intraplate stress. *Int. Geol. Rev.* 45:95–118



# Contents

|  |     |
|--|-----|
| Where Are You From? Why Are You Here? An African Perspective<br>on Global Warming<br><i>S. George Philander</i> .....  | 1   |
| Stagnant Slab: A Review<br><i>Yoshio Fukao, Masayuki Obayashi, Tomoeki Nakakuki,<br/>and the Deep Slab Project Group</i> .....   | 19  |
| Radiocarbon and Soil Carbon Dynamics<br><i>Susan Trumbore</i> .....  | 47  |
| Evolution of the Genus <i>Homo</i><br><i>Ian Tattersall and Jeffrey H. Schwartz</i> .....  | 67  |
| Feedbacks, Timescales, and Seeing Red<br><i>Gerard Roe</i> .....   | 93  |
| Atmospheric Lifetime of Fossil Fuel Carbon Dioxide<br><i>David Archer, Michael Eby, Victor Brovkin, Andy Ridgwell, Long Cao,<br/>Uwe Mikolajewicz, Ken Caldeira, Katsumi Matsumoto, Guy Munhoven,<br/>Alvaro Montenegro, and Kathy Tokos</i> ..... | 117 |
| Evolution of Life Cycles in Early Amphibians<br><i>Rainer R. Schoch</i> .....  | 135 |
| The Fin to Limb Transition: New Data, Interpretations, and<br>Hypotheses from Paleontology and Developmental Biology<br><i>Jennifer A. Clack</i> .....   | 163 |
| Mammalian Response to Cenozoic Climatic Change<br><i>Jessica L. Blois and Elizabeth A. Hadly</i> .....   | 181 |
| Forensic Seismology and the Comprehensive Nuclear-Test-Ban Treaty<br><i>David Bowers and Neil D. Selby</i> .....   | 209 |
| How the Continents Deform: The Evidence from Tectonic Geodesy<br><i>Wayne Thatcher</i> .....   | 237 |
| The Tropics in Paleoclimate<br><i>John C.H. Chiang</i> .....   | 263 |

|  |     |
|--|-----|
| Rivers, Lakes, Dunes, and Rain: Crustal Processes in Titan's Methane Cycle<br><i>Jonathan I. Lunine and Ralph D. Lorenz</i> .....  | 299 |
| Planetary Migration: What Does it Mean for Planet Formation?<br><i>John E. Chambers</i> .....  | 321 |
| The Tectonic Framework of the Sumatran Subduction Zone<br><i>Robert McCaffrey</i> .....  | 345 |
| Microbial Transformations of Minerals and Metals: Recent Advances in Geomicrobiology Derived from Synchrotron-Based X-Ray Spectroscopy and X-Ray Microscopy<br><i>Alexis Templeton and Emily Knowles</i> ..... | 367 |
| The Channeled Scabland: A Retrospective<br><i>Victor R. Baker</i> .....  | 393 |
| Growth and Evolution of Asteroids<br><i>Erik Asphaug</i> .....   | 413 |
| Thermodynamics and Mass Transport in Multicomponent, Multiphase H <sub>2</sub> O Systems of Planetary Interest<br><i>Xinli Lu and Susan W. Kieffer</i> .....   | 449 |
| The Hadean Crust: Evidence from >4 Ga Zircons<br><i>T. Mark Harrison</i> .....   | 479 |
| Tracking Euxinia in the Ancient Ocean: A Multiproxy Perspective and Proterozoic Case Study<br><i>Timothy W. Lyons, Ariel D. Anbar, Silke Severmann, Clint Scott, and Benjamin C. Gill</i> .....                | 507 |
| The Polar Deposits of Mars<br><i>Shane Byrne</i> .....   | 535 |
| Shearing Melt Out of the Earth: An Experimentalist's Perspective on the Influence of Deformation on Melt Extraction<br><i>David L. Kohlstedt and Benjamin K. Holtzman</i> .....                                | 561 |

## Indexes

|   |     |
|---|-----|
| Cumulative Index of Contributing Authors, Volumes 27–37 ..... | 595 |
| Cumulative Index of Chapter Titles, Volumes 27–37 .....       | 599 |

## Errata

An online log of corrections to *Annual Review of Earth and Planetary Sciences* articles may be found at <http://earth.annualreviews.org>